345 E. 47 St., New York, N.Y. 10017

Prediction of the Aerodynamic Environment and Heat Transfer for Rotor-Stator Configurations

L. W. GRIFFIN and H. V. McCONNAUGHEY

Computational Fluid Dynamics Branch
NASA George C. Marshall Space Flight Center
Marshall Space Flight Center, Alabama

ABSTRACT

A numerical study of the aerodynamic and thermal environment associated with axial turbine stages is presented. Computations were performed using a modification of the unsteady viscous code, ROTOR1, and an improved version of the steady inviscid cascade system, MERIDL-TSONIC, coupled with boundary layer codes, BLAYER and STAN5. Two different turbine stages were analyzed: the first stage of the United Technologies Research Center Large Scale Rotating Rig (LSRR) and the first stage of the Space Shuttle Main Engine (SSME) high pressure fuel turbopump turbine. The time-averaged airfoil midspan pressure and heat transfer profiles were predicted for numerous thermal boundary conditions including adiabatic wall, prescribed surface temperature, and prescribed heat flux. Computed solutions are compared with each other and with experimental data in the case of the LSRR calculations. Modified ROTOR1 predictions of unsteady pressure envelopes and instantaneous contour plots are also presented. Relative merits of the two computational approaches are discussed.

NOMENCLATURE

c	Chord
C_p	Coefficient of pressure
c_p	Specific heat, constant pressure
c_v	Specific heat, constant volume
J	Jacobian of coordinate transformation
k	Coefficient of thermal conductivity
p	Pressure
q"	Heat flux
St	Stanton number
T	Temperature
u,v	x and y components of velocity
W	Relative velocity
x	Axial distance
y+	Boundary layer parameter
α	Heat transfer coefficient
μ	Coefficient of viscosity
ρ	Density

SUBSCRIPTS

a	Adiabatic condition
e	Exit condition (averaged across pitch)
r	Relative condition
T	Total (stagnation) quantity
w	Wall quantity
0	Inlet condition (averaged across pitch)
2	Quantity at first row of nodes off boundary

INTRODUCTION

Requirements of increased durability and performance of turbomachines continue to press turbine designers and to demand improvements in the predictive capability of turbine analysis tools. This is especially true in the rocket propulsion arena where increased turbine blade life is essential to the enhancements in reusability required of future rocket propulsion systems. Of importance is the accurate prediction of aerodynamic and thermal loads and the characterization of flow unsteadiness and three-dimensionality.

In the past few years, turbine analysis capabilities have been extended through the development of computational fluid dynamics codes which solve for the unsteady viscous flowfield in an axial turbine stage. Examples of these are presented by Chen (1988), Gibeling, et al. (1988), Jorgenson, et al. (1988), and Rai (1987a, b, c), the pioneering work being that of Rai (1987a). These codes offer the capability to assess the effects of blade row interactions, time and/or space varying inlet profiles, axial gap size, and three-dimensionality [in the case of Chen (1988) and Rai (1987c)] on the flow through a turbine stage. In most cases, the accuracy of these codes has been assessed in terms of time-averaged blade pressure prediction by comparing calculated values with experimental data reported by Dring (1982, 1986c).

The present work is aimed at extending and further evaluating the unsteady codes. Predictive capability is assessed in terms of accuracy of calculated airfoil aerodynamic and thermal loads and in terms of suitability for rocket propulsion applications. Relevant rocket propulsion issues are discussed by Civinskas, et al. (1988). Although only one unsteady code was

Presented at the Gas Turbine and Aeroengine Congress and Exposition—June 4-8, 1989—Toronto, Ontario, Canada

used, it is believed that the qualitative results obtained and issues raised are relevant to most unsteady turbine stage codes. Parallel calculations using conventional steady turbine design analyses were also performed to gauge any improvements in the prediction of time-averaged blade loads using the unsteady approach.

Specifically, the unsteady code ROTOR1 (Rai, 1987a) was modified to incorporate heat transfer prediction capability. The original (adiabatic wall) version and the modified (prescribed blade temperature or prescribed heat flux) versions are applied to the Large Scale Rotating Rig (LSRR) tests performed at United Technologies Research Center (UTRC) by Dring (1986a, b, c) and to the gaseous H_2/H_2O flow in the high pressure fuel turbopump (HPFTP) turbine of the Space Shuttle Main Engine (SSME). For the SSME calculations, various gas properties in ROTOR1 were also changed to better simulate the H_2/H_2O gas mixture in the HPFTP turbine. The same flows were analyzed using an improved version of the steady inviscid quasi-three-dimensional (3D) system MERIDL-TSONIC (Katsanis, 1969, 1977) coupled with boundary layer codes BLAYER (McNally, 1970) and STAN5 (Crawford and Kays, 1976). The time-averaged aerodynamic and thermal blade loads predicted by ROTOR1 are compared with the steady results of MERIDL-TSONIC-BLAYER-STAN5. All calculations associated with the LSRR configuration are compared with the experimental data. In addition, various time-varying features of the flows predicted by ROTOR1 are also presented.

APPLICATION CONFIGURATIONS

The unsteady turbine stage flows which were numerically analyzed are described here. The first is the air flow in the single stage configuration of the UTRC LSRR. The LSRR contains a 5-ft-diameter, single or one-and-one-half stage turbine with average airfoil axial chord of over 15 cm (6 in.). Test conditions corresponding to the calculations presented here involved ambient air entering the turbine at approximately 23 m/s (75 ft/s) corresponding to a flowrate of 18 kg/s (40.3 lbm/s), and the rotor speed was 410 rpm. The turbine model, which has 22 first stage stator vanes and 28 first stage rotor blades, had an axial gap size of 15 percent average axial chord. The rig was run with and without a turbulence generating grid and time-mean aerodynamic and heat transfer measurements were taken. The aerodynamics were not significantly affected by the presence of the grid. On the other hand, the heat transfer profiles measured with the turbulence grid in place were substantially different than those measured with no grid. Additional details are given by Dring (1986a, b, c). The second configuration analyzed is the first stage of the SSME HPFTP turbine. The turbopump is driven by a gaseous hydrogen and steam mixture which, at full power level, enters the turbine at approximately 226 m/s (741 ft/s) and corresponding flow rate of 70 kg/s (154 lbm/s), 1050 K (1900°R), 37,500,000 N/m^2 (5440 $lbf/in.^2$), and the rotor speed is 36,600 rpm. The two-stage turbine has 41 first stage stator vanes and 63 first stage rotor blades with an average axial chord of less than 2.5 cm (1 in.). The axial spacing between first stage stator and rotor is 0.8 cm (0.33 in.). The turbine power is approximately 75,000 hp.

METHOD OF SOLUTION

The flows in the configurations just discussed were numerically analyzed using two different methodologies: an unsteady, viscous stage flow formulation and a steady, inviscid cascade treatment. These are described below.

The two-dimensional (2D) rotor-stator interaction code, ROTOR1, developed by Rai (1987a), simulates the flow through an axial turbine stage by solving the 2D, unsteady, thin-layer Navier-Stokes equations. It features a factored, iterative, implicit algorithm, an Osher upwind differencing scheme, and a Baldwin-Lomax turbulence model. ROTOR1 employs multiple grids. Each blade is surrounded by a fine O-grid which is overlaid onto a coarse H-grid. The H-grids are patched between blade rows, and the rotor H-grid slides past the stationary stator H-grid in time. ROTOR1 is a single-stage code and assumes that blade rows have an equal blade count. Rai (1987a) provides a more detailed description of the ROTOR1 methodology.

The inlet and exit boundary conditions used in this study are the same as those outlined by Rai (1987a) and, thus, are mentioned only briefly here. At the inlet, Riemann invariant R_1 is fixed and Riemann invariant R_2 is extrapolated from the interior. The inlet flow angle is set to zero, and the entropy at the inlet is held constant at the freestream value. A constant static pressure is imposed at the exit.

Three different surface temperature conditions were explored: an adiabatic wall, a prescribed wall temperature, and a prescribed wall heat flux. The no-slip condition and a zero normal pressure gradient along with one of the temperature conditions comprise the surface boundary conditions. Rai (1987a) describes the implementation of these boundary conditions assuming an adiabatic wall. If a nonadiabatic wall is assumed, the wall temperature, T_w, no longer equals T_2, the temperature at the first grid line off of the wall. To implement the surface boundary conditions with this specified wall temperature, the C and D matrices described by Rai (1987a) are replaced by:

$$C = \begin{bmatrix} 1 & 0 & 0 & 0 \\ 0 & 1 & 0 & 0 \\ 0 & 0 & 1 & 0 \\ a & u_w & v_w & 1 \end{bmatrix} \qquad D = \begin{bmatrix} b\theta & -d\theta u_2 & -d\theta v_2 & d\theta \\ 0 & 0 & 0 & 0 \\ 0 & 0 & 0 & 0 \\ a\theta & -\theta u_w & -\theta v_w & \theta \end{bmatrix} \tag{1}$$

where $a = (u_w^2 + v_w^2)/2$, $b = (u_2^2 + v_2^2)/2c_vT_w$, $d = 1/c_vT_w$, and $\theta = -J_2/J_w$.

The capability to calculate heat transfer was added to ROTOR1. The heat transfer was assumed to be due entirely to conduction; therefore, Fourier's law of heat conduction was used, i.e.,

$$q'' = -k\partial T/\partial n \quad . \tag{2}$$

Two types of temperature distribution surrounding the airfoils were considered to approximate the normal derivative of T at the wall. First, the temperature at a blade surface point and at the two closest points along the normal line passing through the surface point was assumed to fit a quadratic polynomial of the form $a+bn+cn^2$, where n is the distance from the surface along the normal line. Next, the temperature distribution was assumed to be linear in n between the boundary point and the first off-boundary point. In both cases, the off-wall point(s) through which the temperature polynomial is fit should lie within the viscous sublayer, i.e., should have a y+ which is no larger than 10. This requires a very fine grid system. For the applications to be discussed in this work, over 25,000 grid points were used and the heat flux was found to be very similar for the two types of interpolation considered.

In addition to the unsteady, high resolution analysis of ROTOR1 just described, an approach more typical of conventional turbine design methodology was used. This consisted of application of the steady, inviscid, quasi-3D plus boundary-layer code, MTSBL, and an improved version of the boundary-layer code STAN5. MTSBL is a composite of improved versions of the codes MERIDL, TSONIC, and BLAYER. It enables an iterative coupling of the quasi-3D flow analysis of MERIDL-TSONIC with the loss calculation in BLAYER. This approach is described by Boyle, et al. (1984). MTSBL and STAN5 were developed and are maintained by NASA Lewis Research Center. Improvements in these codes include the capability to utilize actual mixture properties of gaseous H_2 and steam and the capability in MTSBL to automatically generate an input stream for use with STAN5 for more accurate heat transfer prediction than is available from BLAYER. The heat transfer profile in the leading edge region was approximated using the experimental correlation shown by Civinskas, et al. (1988). The quasi-3D procedure of MTSBL assumes a single blade row. For a stage calculation, then, the converged values of pertinent flow variables at the trailing edge of the first airfoil row are used as the input values for the second airfoil row.

RESULTS AND DISCUSSION

Results generated by the modified ROTOR1 code and by MTSBL and STAN5 are now presented. Aerodynamic results are shown in the form of airfoil pressure coefficients and, in the case of ROTOR1, unsteady pressure envelopes and instantaneous entropy contours. The thermal results are presented in terms of Stanton numbers.

Aerodynamic Results

Plots of calculated and experimentally measured pressure coefficients, defined as

$$C_p = \frac{p - p_{Tr0}}{\frac{1}{2}\rho_0 W_0^2} \qquad (3)$$

are shown in Figures 1 and 2 for the LSRR. The ROTOR1 profiles represent time-averaged (over one period, i.e., one blade pass) values of p, p_{Tr0}, and ρ_0. The agreement between the ROTOR1 predictions and the test data is excellent and is consistent with the results reported by Rai (1987a). The MTSBL predictions for the LSRR stator agree well with the experimental data. However, the LSRR rotor C_p profile computed using MTSBL is low over the latter one-third of the blade on the suction surface.

The pressure coefficients calculated for the first stage of the SSME HPFTP turbine are shown in Figures 3 and 4. Profiles predicted using the two different computational procedures have similar shapes, but the MTSBL predictions are somewhat lower than the ROTOR1 predictions on the stator and are slightly higher on the rotor suction surface. The MTSBL-generated stator C_p profile reflects a higher loss than the ROTOR1 prediction.

Figures 5 through 8 show the unsteady pressure envelopes for the LSRR and HPFTP first stage airfoils calculated by ROTOR1. In both turbines, the effects of rotor-stator interaction, reflected by the amplitude of the pressure variations, are seen to be most significant on the rotor, as is to be expected. Significant effects are also experienced by the LSRR stator as well due to the narrow axial gap of 15 percent axial chord. The relatively more generous axial spacing in the HPFTP minimizes the rotor-stator interaction effects

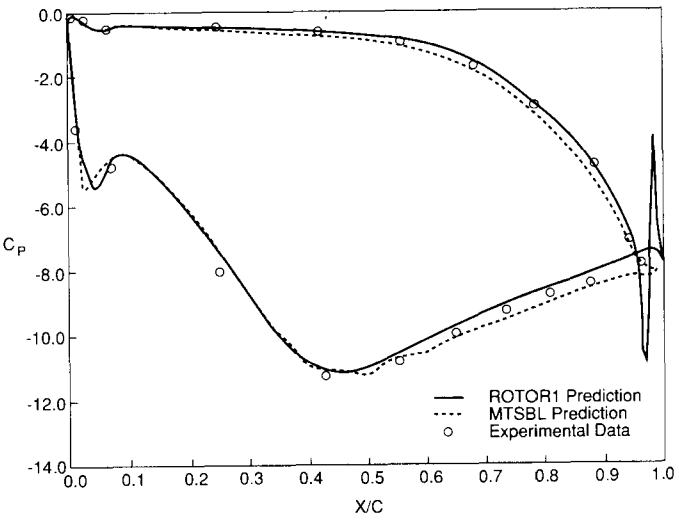

Fig. 1. Pressure Distribution on the LSRR First Stator

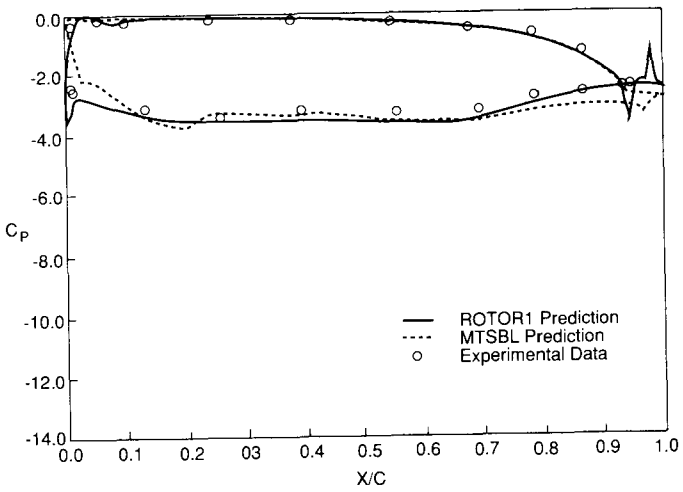

Fig. 2. Pressure Distribution (Relative) on the LSRR Rotor

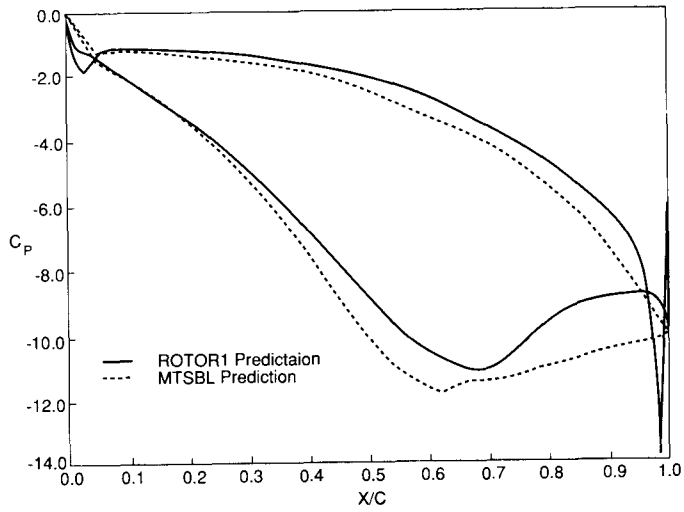

Fig. 3. Pressure Distribution on the SSME HPFTP First Stator

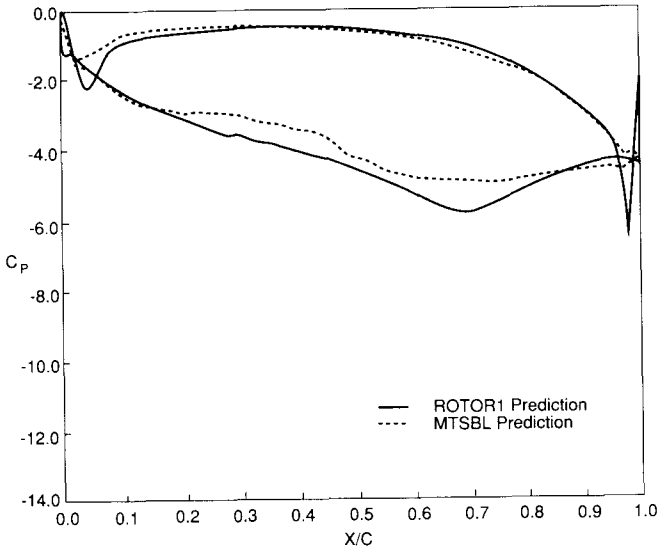

Fig. 4. Pressure Distribution (Relative) on the SSME HPFTP First Rotor

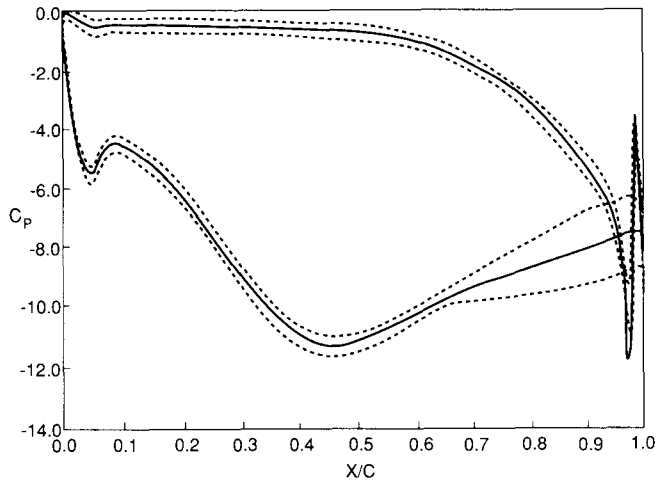

Fig. 5. Unsteady Pressure Envelope of the LSRR First Stator

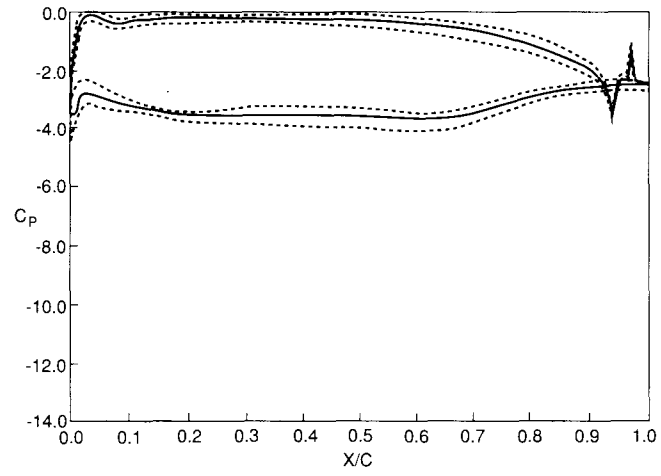

Fig. 6. Unsteady Pressure Envelope of the LSRR Rotor

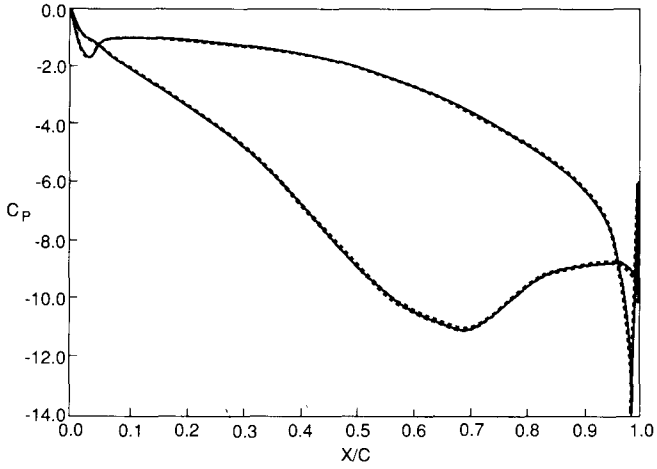

Fig. 7. Unsteady Pressure Envelope of the SSME HPFTP First Stator

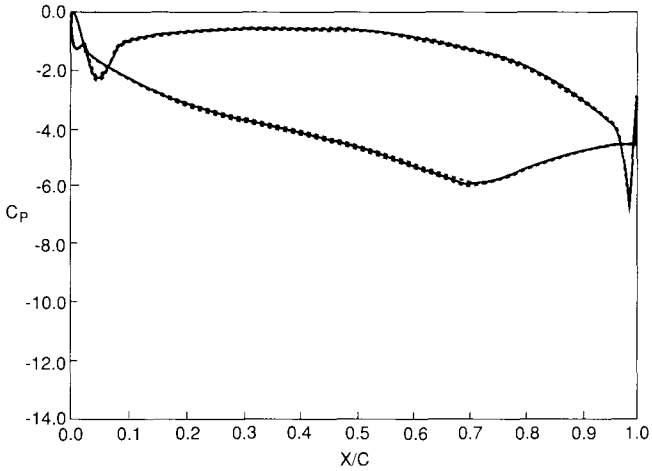

Fig. 8. Unsteady Pressure Envelope of the SSME HPFTP First Rotor

communicated upstream in that turbine. Figure 9 illustrates the flowfield unsteadiness which can be characterized by a ROTOR1 calculation. Instantaneous entropy contours in the HPFTP first stage calculated at four different times within one blade pass are shown. Of interest is the migration of the stator wake fluid through the rotor passage. Similar plots (not shown) reveal the convection of locally hot gas through the turbine stage.

Thermal Results

Stanton numbers for the LSRR and SSME first stages were calculated by ROTOR1 according to the expression

$$St = \frac{q''}{\rho_e W_e c_p (T_a - T_w)} \tag{4}$$

where either q'' or T_w was prescribed and T_a was taken to be the surface temperature profile obtained by a ROTOR1 adiabatic-wall calculation. STAN5 predictions of the Stanton number were based on the definition

$$St = \frac{\alpha}{\rho_e W_e c_p} \tag{5}$$

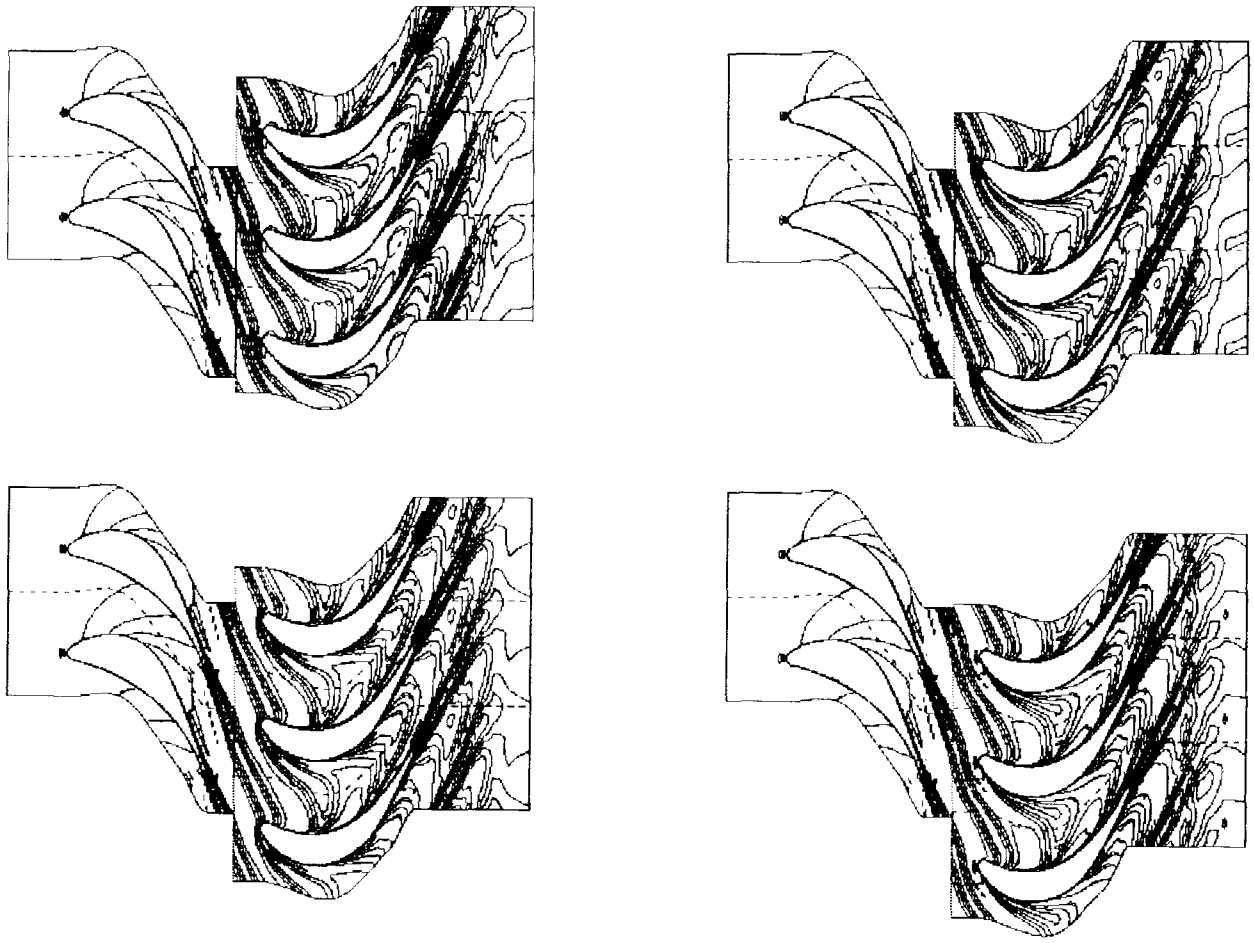

Fig. 9. Instantaneous Entropy Contours at Four Different Times for the SSME HPFTP Turbine (Graphics by D. Goode and J. Ruf)

where the heat transfer coefficient α is output by the code.

Predictions for the LSRR airfoils are shown in Figures 10 and 11 along with the experimental data. Comparison of the stator profiles shows the predictions to be essentially laminar on the pressure surface where the shape of the calculated profiles resembles that of the grid-out measurements. The suction surface calculations, however, incorrectly predict the transition location and yield an altogether incorrect profile shape. The calculated rotor pressure surface profiles appear low and flat as compared to the experimental data. The suction surface profile shape, on the other hand, very closely matches that of the grid-in measurements.

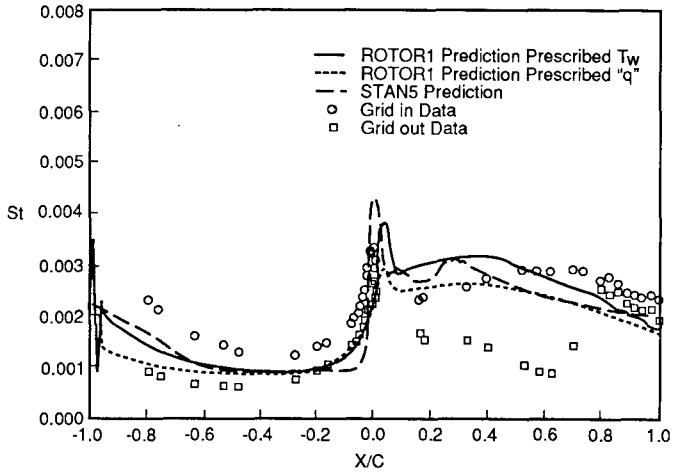

Fig. 10. Comparison of Predicted and Experimental Heat Transfer for the LSRR First Stator

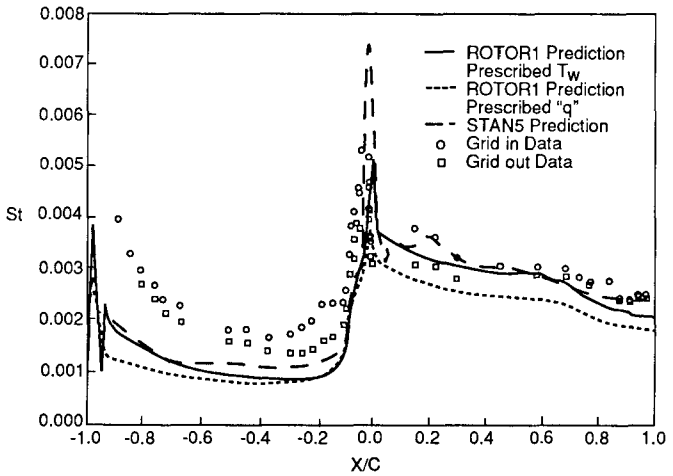

Fig. 11. Comparison of Predicted and Experimental Heat Transfer for the LSRR Rotor

The magnitude of the calculated profile is lower than that measured while the STAN5 rotor suction surface prediction matches the grid-in data remarkably well. These Stanton number predictions are comparable to the analogous numerical results presented by Dring (1987a).

Figures 12 and 13 show Stanton number profiles for the SSME HPFTP first stator and first rotor. The STAN5 results shown correspond to a calculation which incorporated real gas properties associated with a 0.9813 O/F ratio in the upstream preburner and are consistent with results presented by Civinskas, et al. (1988) for the same rotor. A discrepancy between the ROTOR1 and STAN5 predictions is apparent. Which code yields the more correct heat transfer prediction for this case cannot be concluded, however, in light of their more similar profile shapes for the LSRR configuration. One possible source of the disparity in predictions is the ideal-air assumption built into the ROTOR1 code through its calculation of the viscosity μ. In particular, ROTOR1 uses Sutherland's law to calculate μ and uses constants appropriate for air. But Sutherland's law is not valid for the SSME HPFTP gas mixture for any Sutherland's constant. Incorporation of real gas properties into the modified ROTOR1 code is now underway at NASA Marshall Space Flight Center (MSFC) to correct the ideal-air assumptions inherent in the original code.

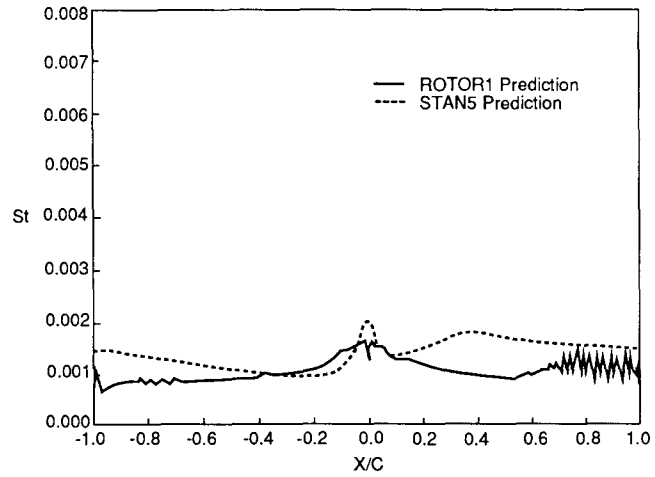

Fig. 12. Comparison of ROTOR1 and STAN5 Heat Transfer Predictions for the SSME HPFTP First Stator

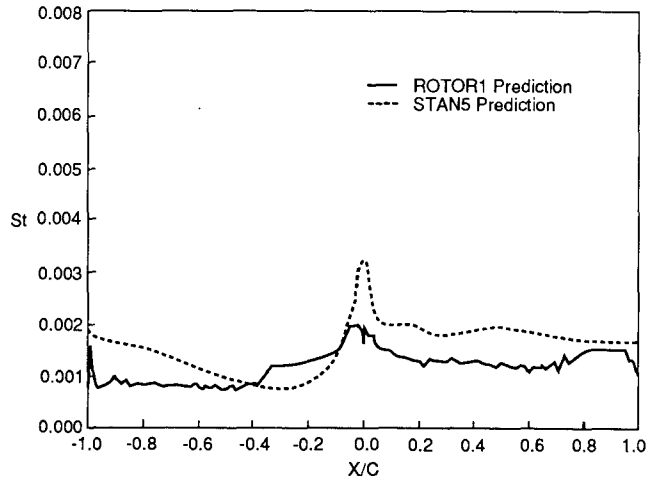

Fig. 13. Comparison of ROTOR1 and STAN5 Heat Transfer Predictions for the SSME HPFTP First Rotor

Resource Requirements

All calculations were performed on the CRAY X-MP 416 at MSFC. The MTSBL runs each required between five and six CPU minutes and approximately 900,000 words of memory. The heat transfer predictions obtained with STAN5 and leading edge correlations required less than two CPU minutes and 400,000 words of memory. The ROTOR1 analysis is naturally more computer intensive due to its high spatial resolution and its unsteady formulation. A ROTOR1 calculation started from free-stream conditions requires six CPU hours to reach temporal periodicity and 2,100,000 words of core memory plus 800 sectors of SSD.

CONCLUSIONS

In summary, a numerical study of the aerodynamic and thermal environment associated with axial turbine stages was conducted to assess the merits of unsteady stage codes. The particular unsteady code used in this study was ROTOR1. Parallel calculations using codes employing conventional steady turbine design methodology, MTSBL and STAN5, were performed to measure any improvements in prediction of time-averaged blade loads using the unsteady approach. The codes were applied to two different turbine stages: the first stage of the UTRC LSRR and the SSME HPFTP turbine.

Both the time-averaged pressure distributions of ROTOR1 and the steady pressure distributions of MTSBL compare well with experimental data. The STAN5 heat transfer predictions for the LSRR are similar to the ROTOR1 predictions, although the STAN5 prediction for the rotor suction surface better matches the data. Qualitatively, both the STAN5 and the ROTOR1 heat transfer profiles exhibit reasonable agreement with the data, except on the stator suction surface where neither code correctly predicts the transition location or profile shape. The magnitude of the Stanton number is somewhat low, especially when a constant heat flux condition is used in ROTOR1. The heat transfer predicted by ROTOR1 for the SSME HPFTP turbine does not compare well with the STAN5 results. The discrepancy may be due to the ideal-air assumption used in the calculation of viscosity in ROTOR1 which is likely to yield erroneous heat transfer results when air is not the working fluid. If the unsteady codes are to predict heat transfer to some degree of accuracy in other than air-driven turbines, this assumption must be changed.

Both approaches yield similar time-averaged or steady-state aerodynamic and thermal results. Therefore, it only time-averaged quantities are needed, the conventional, steady turbine design methodology is the preferred approach since it requires so much less time and computer resources as compared to the unsteady approach but produces comparable results. On the other hand, if characterization of the unsteady nature of flow through an axial turbine is also required, the unsteady codes constitute the natural approach.

ACKNOWLEDGMENTS

The authors wish to acknowledge the important contributions to this work made by colleagues Bob Boyle and Kaz Civinskas of NASA Lewis Research Center through the sharing of their knowledge of MTSBL and STAN5 operation and of turbine analysis in general. The authors are also grateful to Bob Dring, Mike Blair, and Roger Davis of UTRC, and to Om Sharma of Pratt and Whitney for valuable discussions related to turbine heat transfer which stimulated some of the work reported here. A portion of this work was done under Contract NAS8-36284 while the first author was employed by Lockheed Missiles and Space Company.

which stimulated some of the work reported here. A portion of this work was done under Contract NAS8-36284 while the first author was employed by Lockheed Missiles and Space Company.

REFERENCES

Boyle, R. J., et al., 1984, "Comparison Between Measured Turbine Stage Performance and the Predicted Performance Using Quasi-3D Flow and Boundary Layer Analyses," NASA TM 83640.

Chen, Y. S., 1988, "3-D Stator-Rotor Interaction of the SSME," AIAA Paper No. 88-3095.

Civinskas, K. C., et al., 1988, "Impact of ETO Propellants on the Aerothermodynamic Analyses of Propulsion Components," AIAA Paper No. 88-3091.

Crawford, M. E. and Kays, W. M., 1976, "STAN5 - A Program for Numerical Computation of Two-Dimensional Internal and External Boundary Layer Flows," NASA CR-2742.

Dring, R. P., et al., 1982, "Turbine Rotor-Stator Interaction," Journal of Engineering for Power, Vol. 104, pp. 729-742.

Dring, R. P., et al., 1986, "The Effects of Inlet Turbulence and Rotor/Stator Interactions on the Aerodynamics and Heat Transfer of a Large-Scale Rotating Turbine Model, Vol. I: Final Report," NASA CR 4079.

Dring, R. P., et al., 1986, "The Effects of Inlet Turbulence and Rotor/Stator Interactions on the Aerodynamics and Heat Transfer of a Large-Scale Rotating Turbine Model, Vol. II: Heat Transfer Data Tabulation, 15% Axial Spacing," NASA CR 179469.

Dring, R. P., et al., 1986, "The Effects of Inlet Turbulence and Rotor/Stator Interactions on the Aerodynamics and Heat Transfer of a Large-Scale Rotating Turbine Model, Vol. IV: Aerodynamic Data Tabulation," NASA CR 179469.

Gibeling, H. J., et al., 1988, "An Implicit Navier-Stokes Analysis of Turbine Rotor-Stator Interaction," AIAA Paper No. 88-3090.

Jorgenson, P. C. E. and Chima, R. V., 1988, "An Explicit Runge-Kutta Method for Unsteady Rotor Stator Interaction," AIAA Paper No. 88-0049.

Katsanis, T., 1969, "FORTRAN Program for Calculating Transonic Velocities on a Blade-to-Blade Stream Surface of a Turbomachine," NASA TN D-5427.

Katsanis, T. and McNally, W. D., 1977, "Revised FORTRAN Program for Calculating Velocities and Streamlines on the Hub-Shroud Midchannel Stream Surface of an Axial-, Radial-, or Mixed-Flow Turbomachine or Annular Duct, Vol. I - User's Manual," NASA TN D-8430.

McNally, W. D., 1970, "FORTRAN Program for Calculating Compressible Laminar and Turbulent Boundary Layers in Arbitrary Pressure Gradients," NASA TN D-5681.

Rai, M. M., 1987, "Navier-Stokes Simulations of Rotor-Stator Interaction Using Patched and Overlaid Grids," Journal of Propulsion and Power, Vol. 3, No. 5, pp. 387-396.

Rai, M. M., 1987, "Navier-Stokes Analyses of the Redistribution of Inlet Temperature Distortions in a Turbine," AIAA Paper No. 87-2146.

Rai, M. M., 1987, "Unsteady Three-Dimensional Navier-Stokes Simulations of Turbine Rotor-Stator Interaction," AIAA Paper No. 87-2058.